Aerosol and Air Quality Research, 20: 862–876, 2020

ISSN: 1680-8584 print / 2071-1409 online
doi: 10.4209/aaqr.2019.11.0596

Application of Rice Straw, Corn Cob, and Lotus Leaf as Agricultural Waste Derived Catalysts for Low Temperature SCR Process: Optimization of Preparation Process, Catalytic Activity and Characterization

Chenglong Yu[1*], Huaijian Wang[1], Meijuan Lu[1], Fangxu Zhu[2], Yue Yang[3], Hong Huang[4], Changwei Zou[4], Jiangbo Xiong[1], Zhiyong Zhong[1]

[1] *School of Land Resources and Environment, Jiangxi Agricultural University, Nanchang 330045, China*
[2] *No.270 Research Institute of Nuclear Industry, Nanchang 330200, China*
[3] *Department of Life Food Science and Technology Environmental Engineering, Yangjiang Polytechnic, Yangjiang 529500, China*
[4] *School of Resources, Environment and Chemical Engineering, Nanchang University, Nanchang 330031, China*

ABSTRACT

Carbon-based catalytic materials have received significant attention for low temperature flue gas denitrification ($DeNO_x$) process, due to their physicochemical properties and ease of modification. To improve the $DeNO_x$ efficiency, preparation of biochar catalyst supports was conducted that included the acid treatment of the agricultural wastes rice straw, corn cobs and lotus leaves. Taguchi experimental design (3^4) was employed to screen suitable carbon materials and optimize the preparation parameters of the biochar. All of the acid-modified and unmodified samples were evaluated to determine their performance and they were characterized by using SEM, BET and FT-IR analysis. The experimental and characterization results showed that acid modification of the biochars improved their $DeNO_x$ performance, which may have been due to the changes in the physical and chemical properties of the carbon material following the acid treatment. The optimum combination in the acid modification procedure was found to be the use of lotus leaf carbon treated with an acid/mass ratio of 1.50 and a pyrolysis temperature of 800°C. The biochar prepared using these optimum preparation parameters were then employed as a carrier to support an active catalyst component (MnO_x). The lotus leaf biochar supported 10 wt% manganese catalyst prepared using ultrasonic impregnation method exhibited nearly 90% NO_x conversion at 250°C at a high space velocity of 45, 000^{-1}, and it exhibited strong resistance to H_2O. Additional studies showed that higher redox capacity and suitable surface acidity were two of the deciding factors in the improved low temperature SCR performance of the 10% Mn/LBC catalysts.

Keywords: Agricultural wastes; Acid modification; Low temperature flue gas denitrification; Carbon materials.

INTRODUCTION

Nitrogen oxides (NO_x) generated by fossil fuel combustion can produce a number of environmental problems, including urban haze, photo-chemical smog, acid rain, ozone depletion and greenhouse effects (Anenberg *et al.*, 2012; Cheng *et al.*, 2018; Huang *et al.*, 2019; Mu *et al.*, 2019). Fossil fuel combustion emissions of NO_x from industrial and residential energy consumption over the last century have been the primary source of NO_x in the atmosphere (Skalska *et al.*, 2010). In addition, severe urban haze has recently become of the most significant urban air quality issues, and NO_x has been shown to be one of the most important precursors of this haze pollution (Anenberg *et al.*, 2012). Consequently, removal of NO_x from industrial flue gas has become an increasingly urgent task to improve urban ambient air quality (Skalska *et al.*, 2010; Anenberg *et al.*, 2012; Wang and Hao, 2012). Several techniques have been used for the elimination of NO_x from flue gas including selective catalytic reduction (SCR), catalytic decomposition, liquid absorption and plasma catalysis. However, of these, SCR of NO_x by NH_3 is one of the most effective flue gas cleaning technologies for stationary sources. The V_2O_5-WO_3/TiO_2 commercial catalysts that form the basis of SCR technology have been widely studied and the SCR unit is always situated in front of the dust precipitation and desulphurization units in a treatment system (Bosch, 1988; Busca *et al.*, 1998; Chen *et al.*, 2018). The high operating temperature of 300–450°C and the toxicity of vanadium, limit its practical application as a commercial catalyst for industrial

* Corresponding author.
E-mail address: chenglongyu888@163.com

furnaces that emit low temperature flue gases (< 250°C). This includes the coking industry, refuse incineration and coal-fired power plants (Li *et al.*, 2011; Fu *et al.*, 2014). Therefore, the necessity has developed to identify vanadium-free low temperature SCR catalysts that can be used to lower the NO_x emissions in these industries.

Carbon materials, including activated carbon, graphene, carbon nanotubes etc., have found wide application for use in low temperature SCR, because of their high specific surface areas and chemical stability (Marban *et al.*, 2004; Lu *et al.*, 2010; Zhu *et al.*, 2011; Wang *et al.*, 2012; Jiao *et al.*, 2015; Yu *et al.*, 2015). In particular, the manganese oxide catalysts have attracted great attention, because they contain various types of labile oxygen and oxidation states of Mn (Jiang *et al.*, 2019b; Zhang *et al.*, 2019; Tong *et al.*, 2020; Wang *et al.*, 2020). This improves the feasibility of the use of these catalysts to complete the catalytic cycle in low temperature NH_3-SCR. Therefore, the combination of MnO_x and carbon materials could produce an ideal low temperature SCR catalyst. Moreover, many carbon-based low temperature SCR catalysts have been developed over the past 10 years that offer high low temperature SCR performance, but also have good anti-poisoning properties due to the hydrophobicity and special pore structure of carbon materials (Bai *et al.*, 2010; Xiao *et al.*, 2016; Yu *et al.*, 2016; Dong *et al.*, 2017). However, the high cost of these carbon materials continues to be the main impediment to their widespread use in NO_x removal processes (Zhu *et al.*, 1999; Huang and Teng, 2003). Carbon materials can be easily produced as pellets, which are cheaper to produce than honeycomb-shaped one. Therefore, the challenge has been to find a cheaper carbon support for the SCR catalyst and then modify it to enhance its SCR catalytic performance. To date, its environmental benefits and abundance have convinced many researchers to devote their efforts to the production of activated carbon or other useful materials from various types of biomass (Jo *et al.*, 2011), such as cotton stalks (Shen *et al.*, 2015), peanut shell (Yang *et al.*, 2018), rice straw (Cha *et al.*, 2010), rice husk (Chen *et al.*, 2019), etc. However, there have been few reported studies that have focused on the modification and optimization of the preparation of biochar from agricultural waste. Using agricultural wastes for biomass energy recovery and air pollution control could also help to solve the problem of disposing of these agricultural wastes.

It has been found that a change in surface chemistry of modified carbonaceous materials affects their adsorption and catalytic properties (Boehm, 2002). Samojeden *et al.* (Samojeden *et al.*, 2015) provided an overview of how to enhance $DeNO_x$ performance of the carbon materials. A study reported by Zhou *et al.* (2007) also found that the HNO_3-modified AC could increase the abundance of various oxygen containing functional groups on the carbon surface, which was beneficial to the $DeNO_x$ reaction. Hence, it appears to be very important to modify the raw biochar materials to enhance their $DeNO_x$ properties. However, the type of raw material and its nature also dictate the $DeNO_x$ activity of resulting biochars (Cha *et al.*, 2010; Ahmad *et al.*, 2016). In addition, the nature and internal structure of the raw materials can affect the catalytic activity of the prepared biochar-based catalysts. Thus, a comparative study of the preparation and modification of the various types of raw biomass charcoal is needed.

In this reported work, Taguchi experimental design (3^4) was employed to screen suitable carbon materials and optimize the preparation parameters of the biochar materials. In addition, the effect of acid modification on the low temperature flue gas $DeNO_x$ performance of these biochars was also studied. Moreover, the low temperature SCR performance of various raw biomass charcoals used in preparing MnO_x supported catalysts was determined and the related structure-activity relationship between these materials was also investigated.

EXPERIMENTAL

Orthogonal Design of Catalysts

A Taguchi's orthogonal array L9 was used for selection of the raw carbon materials and the methods for their modification. In this reported study, the carbon material type, pyrolysis temperature, acid type and dosage of acid were used as factors in orthogonal experiments. Each factor was set to three levels and an orthogonal table L9 (3^4) of was designed. Table 1 shows the various test factors and selected levels. Factor A was the carbon material type, which was either the rice straw, corn cob or lotus leaf. These starting materials were obtained from the experimental agricultural fields of Jiangxi Agricultural University. Factor B was the pyrolysis temperature for the preparation of the biochar, which was 600°C, 700°C and 800°C. Factor C was the type of acid used, which included nitric acid, phosphoric acid or sulphuric acid. Factor D was mass ratio of acid to raw material, which was 0.75, 1.50 and 3.00. This experimental design reduced the number of runs needed to screen the candidate catalysts or catalyst supports from 27 runs to 9 runs.

Catalysts Preparation

For comparison, three kinds of the biomass char were obtained from rice straw, corn cob and lotus leaf. All of the starting materials were dried for 12.0 h at 110°C and then pyrolyzed at a specified temperature for 2.0 h in a nitrogen atmosphere. The three carbon materials (rice straw, corn cob and lotus leaf) were then ground and sieved through 20–40 mesh screens, followed by washing with distilled water 5 times and drying at 110°C for 5.0 h. These three samples constituted the unmodified materials and were labeled CK. 1, CK. 2 and CK. 3. Proximate and ultimate analyses were also conducted using three kinds of agricultural waste (rice straw, corn cob and lotus leaf) as shown in Table 2.

In this experiment, Cat. 1 to Cat. 9 represent the acid modified samples. With the exception of the acid modification, all of the procedures used for the preparation of biochars were the same for the modified and unmodified material. The mass ratio of acid to biomass material for the modified samples was designated as x: 1 with x = 3.00, 1.50, 0.75. The acid modified samples were dispersed in a specific acid solution and stirred for 2.0 hours and completely impregnated the biochar with acid for 14.0 hours and then the material was filtered from solution. The filtered powders were dried at 105°C for 24.0 hours, and calcined in a tube resistance

Table 1. Orthogonal experimental design of acid modification experiments.

Factors	A (Carbon material type)	B (Pyrolysis temperature/°C)	C (Acid type)	D (Dosage of acid/mass ratio)
Level				
Level 1	Rice straw	600	Nitric acid	0.75
Level 2	Corn cob	700	Phosphoric acid	1.50
Level 3	Lotus leaf	800	Sulphuric acid	3.00
Catalysts				
Cat. 1	Rice straw	600	Nitric acid	0.75
Cat. 2	Rice straw	700	Phosphoric acid	1.50
Cat. 3	Rice straw	800	Sulphuric acid	3.00
Cat. 4	Corn cob	600	Phosphoric acid	3.00
Cat. 5	Corn cob	700	Sulphuric acid	0.75
Cat. 6	Corn cob	800	Nitric acid	1.50
Cat. 7	Lotus leaf	600	Sulphuric acid	1.50
Cat. 8	Lotus leaf	700	Nitric acid	3.00
Cat. 9	Lotus leaf	800	Phosphoric acid	0.75

Table 2. Proximate analysis and ultimate analysis of raw material.

Sample	Proximate analysis (wt%)				Ultimate analysis (wt%)			
	Water	Ash	Volatiles	Fixed carbon	C	H	N	O and others
Rice straw	6.80	12.78	66.84	13.58	37.50	5.10	1.40	56.00
Corn cob	4.90	2.94	76.02	16.14	42.90	6.00	1.00	50.10
Lotus leaf	10.01	7.59	65.54	16.86	45.70	5.80	3.50	45.00

furnace at y°C (y = 600, 700, 800) for 2.0 h using a ramp rate of 5°C min^{-1} in N_2 atmosphere. After the activation, N_2 was continuously flowed through the furnace until the tube furnace tube reached room temperature to obtain the primary biochar product. Then, the samples were washed with deionized water until the wash water was neutral pH, and the washed samples were dried at 105°C. The final powders were used as the prepared biochar or biochar carriers in this study.

A series of z wt%/RBC, z wt%/CBC and z wt%/LBC catalysts (z = 0, 5, 10, 15) were prepared using the ultrasonic impregnation method. RBC, CBC and LBC represented rice straw biochar, corn cob biochar and lotus leaf biochar. A solution of manganese acetate was made with a constant Mn loading of z wt%. This solution was then added to a beaker containing an individual biochar. This mixture was sonicated for 0.5 h to affect complete dispersion of the biochar in the solution. After Mn impregnation, the samples were dried in air at 100°C for 12 h, and then calcined in a tubular furnace in N_2 at 400°C for 2 h. The specific preparation parameters of these catalysts are shown in Table 3.

NH_3-SCR Activity Measurement

The activity tests of the samples were performed in a fixed-bed quartz flow reactor at atmospheric pressure. A 40–60 mesh sample (1.6 mL) was placed in a fixed-bed quartz reactor (12 mm i.d. × 600 mm in length), and the reaction temperature was increased from 100°C to 300°C at a ramp rate of 5°C min^{-1}. The feed gas composition was 0.06% NO, 0.06% NH_3, 2.5% O_2, 8.0 % H_2O (when used), balanced with Ar. The total flow rate was 1200 mL min^{-1}, which corresponded to a space velocity (GHSV) of 45,000 h^{-1}. The composition of the product gas was continually monitored using a Testo 350 NO-NO_2-NO_x flue gas analyzer (Testo Limited, Germany). The NO_x removal efficiency was calculated using the following equations:

$$\mathrm{NO}_x \text{ conversion } \% = 100 \times \frac{\left(C^{in}_{\mathrm{NO}_x} - C^{out}_{\mathrm{NO}_x}\right)}{C^{in}_{\mathrm{NO}_x}} \quad (1)$$

where the subscripts "C^{in}" and "C^{out}" represent the inlet and outlet gas concentrations of NO_x, respectively.

Characterization of Catalysts

The morphology of the catalyst samples was studied using scanning electron microcopy (SEM) employing a HITACHI S-3400N instrument. The BET surface areas of the catalysts were measured using a Micromeritics ASAP 2020 analyzer (Micromeritics Instrument Corp., USA). The FT-IR spectra of the biochar samples were recorded using a Nicolet 6700 FTIR spectrometers and the FTIR spectra were obtained at a resolution of 4 cm^{-1}.

RESULTS AND DISCUSSION

SCR Catalytic Activity

The use of biochars derived from rice straw, corn cob and lotus leaf, which are normally disposed of as agricultural waste, was investigated as potential catalysts for low temperature selective catalytic reduction of NO_x by NH_3. Three kinds of biochars were prepared using these three precursors employing a designed orthogonal experiment (see Table 1). As seen in Fig. 1, the NO_x conversions of the

Table 3. The specific preparation parameters of these catalysts

Factors	A (Carbon material type)	B (Pyrolysis temperature/°C)	C (Acid type)	D (Dosage of acid/mass ratio)	Theoretical loading of active components
Control Group Catalysts					
CK. 1	Rice straw	700	-	-	-
CK. 2	Corn cob	700	-	-	-
CK. 3	Lotus leaf	700	-	-	-
Optimized Catalysts					
OP. 1 (Pure RBC)	Rice straw	800	Nitric acid	1.50	0
OP. 2 (Pure CBC)	Corn cob	800	Nitric acid	1.50	0
OP. 3 (Pure LBC)	Lotus leaf	800	Nitric acid	1.50	0
10%Mn/RBC	Rice straw	800	Nitric acid	1.50	10% Mn
10%Mn/CBC	Corn cob	800	Nitric acid	1.50	10% Mn
10%Mn/LBC	Lotus leaf	800	Nitric acid	1.50	10% Mn
5%Mn/LBC	Lotus leaf	800	Nitric acid	1.50	5% Mn
15%Mn/LBC	Lotus leaf	800	Nitric acid	1.50	15% Mn

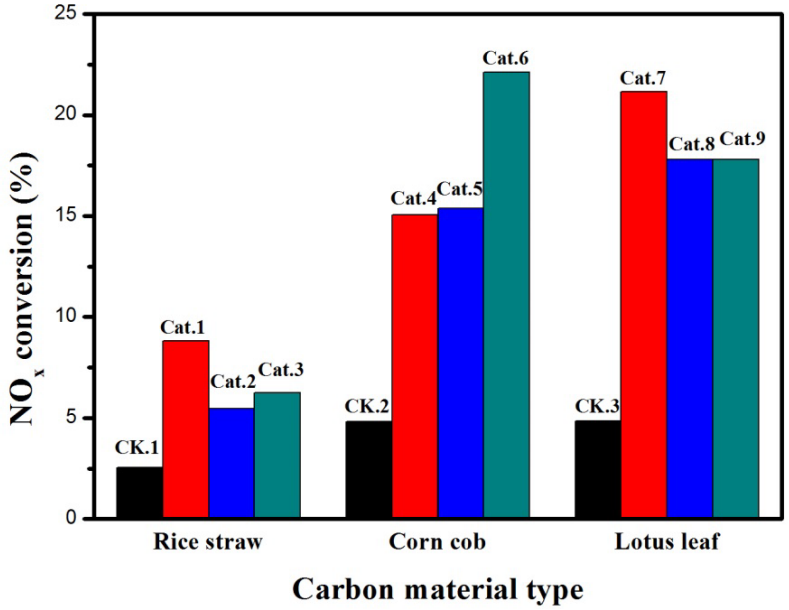

Fig. 1. NO_x removal rate of these biochars before and after acid modification; Reaction conditions: 0.06% NO, 0.06% NH_3, 2.5% O_2, Ar balance, 150°C.

unmodified samples CK. 1, CK. 2 and CK. 3 were all lower than 5% at a reaction temperature of 150°C, and the $DeNO_x$ activity of the unmodified samples (CK.1–CK.3) was also much lower than that of the modified samples (Cat. 1–Cat. 9). The NO_x conversion rate of the acid modified carbon materials was significantly higher than that of the unmodified samples, indicating that the physicochemical properties of the carbon materials was altered by the acid modification process. This phenomenon was consistent with the research reported of Ren *et al.* (2017) and Shen *et al.* (2015). The NO_x conversion of the acid modified rice straw biochar was lower than that of the other two kinds of acid modified bichar, which was less than 10%. However, the NO_x conversion by the acid modified lotus leaf biochar was more than 17% greater, and overall level of the $DeNO_x$ rates of these biochars was relatively high. The optimum result of 21.0% conversion by the lotus leaf biochar was obtained using Cat. 7, which was processed using sulphuric acid. However, of the 12 sets data shown in Fig. 1, Cat. 6 (corn cob), which was prepared at 800°C using nitric acid, exhibited the best $DeNO_x$ result. These data together with the variable analysis of the orthogonal experiments can provide the optimum preparation parameters of the biochar material for flue gas $DeNO_x$ at low temperature. A detailed analysis of this process is included in Section 3.2.

Variance Analysis of the Orthogonal Experiments

Based on the of the activity evaluation, an orthogonal test method was used to determine the effect of carbon material type, pyrolysis temperature, acid type and weight ratio (acid/raw material) on the $DeNO_x$ rate of prepared biochar materials. Each of the samples was tested at three levels and orthogonal experiments L9 (3^4) were used to screen the optimum preparation parameters for producing the biochar.

The orthogonal experimental results are shown in Table 4. As can be seen from these data, the $DeNO_x$ rates of the corn cob biochar and lotus leaf biochar were higher than the results obtained using the rice straw biochar. The maximum $DeNO_x$ rate for rice straw biochar was 8.81%, the minimum $DeNO_x$ rates of the corn cob bio-char and the lotus leaf biochar were 15.06% and 17.79% respectively. The $DeNO_x$ rate of all the rice straw bio-char samples was very low, which may have been related to the large amount of inert Si in these samples. The highest $DeNO_x$ rates for the three carbon materials (rice straw, corn cob and lotus leaf) were 8.81%, 22.12% and 21.15%, respectively. This indicated that lotus leaf bio-char or related derived catalysts exhibited good potential for application in a low temperature flue gas $DeNO_x$ process.

The range analysis results for the $DeNO_x$ rate are listed in Table 5. The value of the range of Factor A (carbon material type) was 36.22, which was the maximum of the four factors. The second highest was Factor C (acid type) with a value of 10.42. The third was Factor D (dosage) had a value of 9.62. Therefore, the order of the influencing factors on the $DeNO_x$ rate in sequence was A > C > D > B. For Factor A, A3 with a value of 56.73 was optimum, C1 was best a value of 48.72, D2 was best with a value of 48.72 and B3 was best with a value 46.16 was optimum for $DeNO_x$ rate, respectively (see Fig. 2). The variance analysis results are provided in Table 6. The F values for Factor A, Factor B, Factor C and Factor D were 23.77, 1.00, 1.65 and 1.47, respectively. When the Significance $\alpha = 0.05$, $F_A > F_{0.05}(2, 2) = 19$. Therefore, Factor A was the most significant in the $DeNO_x$ rate and the impact of Factor B, C and D on the $DeNO_x$ rate of the biochar material was very limited. The variance analysis results were in agreement with the results of the range analysis. For acid modification, the optimum combination for the $DeNO_x$ experimental was A3C1D2B3, in other words, lotus leaf carbon material, nitric acid, an acid/mass ratio of 1.50 and a pyrolysis temperature of 800°C.

Characterization of the Biochar

SEM Analysis

Fig. 3 shows the SEM micrographs of rice straw samples with and without acid modification. The effect of acid modification on the surface morphology of the straw biochar was quite obvious. The CK. 1 sample (Figs. 3(a) and 3(b)) was also prepared by pyrolysis at 700°C under N_2 atmosphere conditions with no acid modification. As can be seen in this micrograph, impurities and fragments are present on the non-acid modified rice straw biochar materials, which appeared bar-like or wire-like shapes. This phenomenon was also reported by Peng *et al.* (Peng *et al.*, 2011). Following acid modification, the surface morphology of the acid modified rice straw biochar (Cat. 1; Figs. 3(c) and 3(d)) was more regular than the non-acid modified sample. In addition, the SEM images revealed that the biochar consisted of irregular spherical bulges with a porous structure, which provided effective catalyst adsorption sites. Considering that its $DeNO_x$ performance was improved after acid modification, it was concluded that the small spherical bulges on the biochar surface may have been the reason for the improvement in the catalytic activity of the material.

Fig. 4 shows the SEM micrographs of the corn cob samples before and after acid modification. The CK. 2 biochar sample (Figs. 4(a) and 4(b)) was prepared by pyrolysis at 700°C under N_2 atmosphere conditions. The surface of this sample appears to have very few channels with significant amounts of debris on the surface. Figs. 4(c) and 4(d) are SEM micrographs of the corn cob biochar material, which appears to show an ordered honey-comb structure of macropores measuring 5–15 μm in diameter, separated by relatively

Table 4. Orthogonal results of acid modification.

Experiment no.	A (Carbon material type)	B (Pyrolysis temperature/°C)	C (Acid type)	D (Dosage of acid/mass ratio)	$DeNO_x$ rate (%)
Cat. 1	Rice straw	600	Nitric acid	0.75	8.81
Cat. 2	Rice straw	700	Phosphoric acid	1.50	5.45
Cat. 3	Rice straw	800	Sulphuric acid	3.00	6.25
Cat. 4	Corn cob	600	Phosphoric acid	3.00	15.06
Cat. 5	Corn cob	700	Sulphuric acid	0.75	15.38
Cat. 6	Corn cob	800	Nitric acid	1.50	22.12
Cat. 7	Lotus leaf	600	Sulphuric acid	1.50	21.15
Cat. 8	Lotus leaf	700	Nitric acid	3.00	17.79
Cat. 9	Lotus leaf	800	Phosphoric acid	0.75	17.79

Table 5. Range analysis results of $DeNO_x$ rate.

Index	A (Carbon material type)	B (Pyrolysis temperature/°C)	C (Acid type)	D (Dosage of acid/mass ratio)
K1	20.51	45.02	48.72	41.98
K2	52.56	38.62	38.30	48.72
K3	56.73	46.16	42.78	39.10
Range	36.22	7.54	10.42	9.62
Range size	A > C > D > B			
Optimal scheme	A3C1D2B3			

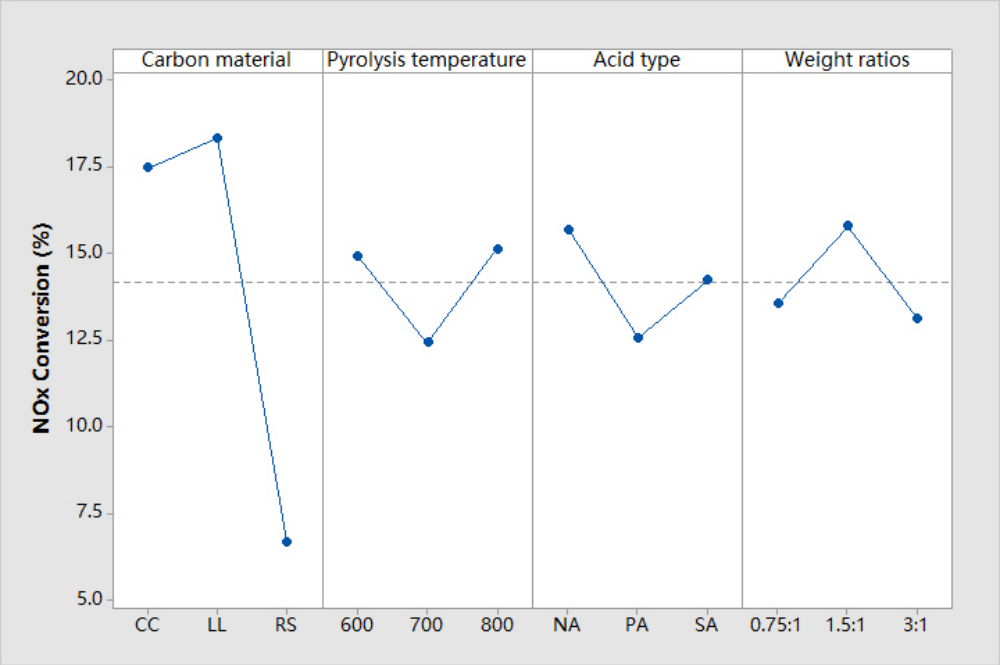

Fig. 2. Effect of each design parameter on the $DeNO_x$ rate; "CC" refers to corn cob, the "LL" refers to lotus-leaf, "RS" refers to rice straw, "NA" refers to nitric acid, "PA" refers to phosphoric acid and "SA" refers to sulphuric acid.

Table 6. Variance analysis results of $DeNO_x$ rate.

Variance source	Deviance quadratic sum	Degree of freedom	Mean square	F value
A	261.83	2	130.91	23.77
B	11.01	2	5.50	1.00
C	18.21	2	9.10	1.65
D	16.25	2	8.12	1.47
Error	11.01	2		
Total	307.30	8		

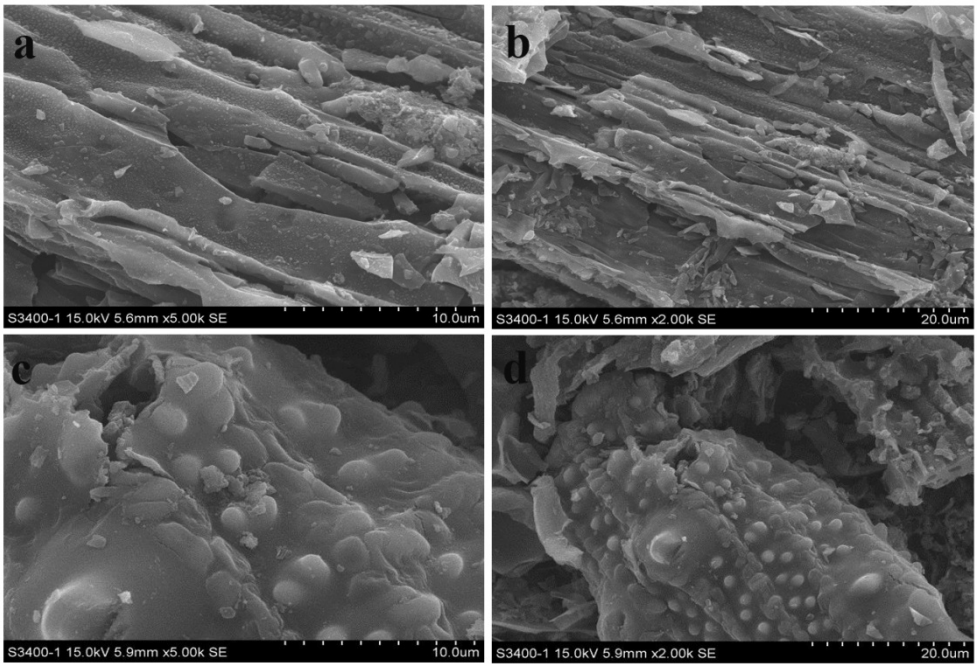

Fig. 3. SEM images of selected rice straw biochar; CK. 1: (a) and (b), Cat. 1: (c) and (d).

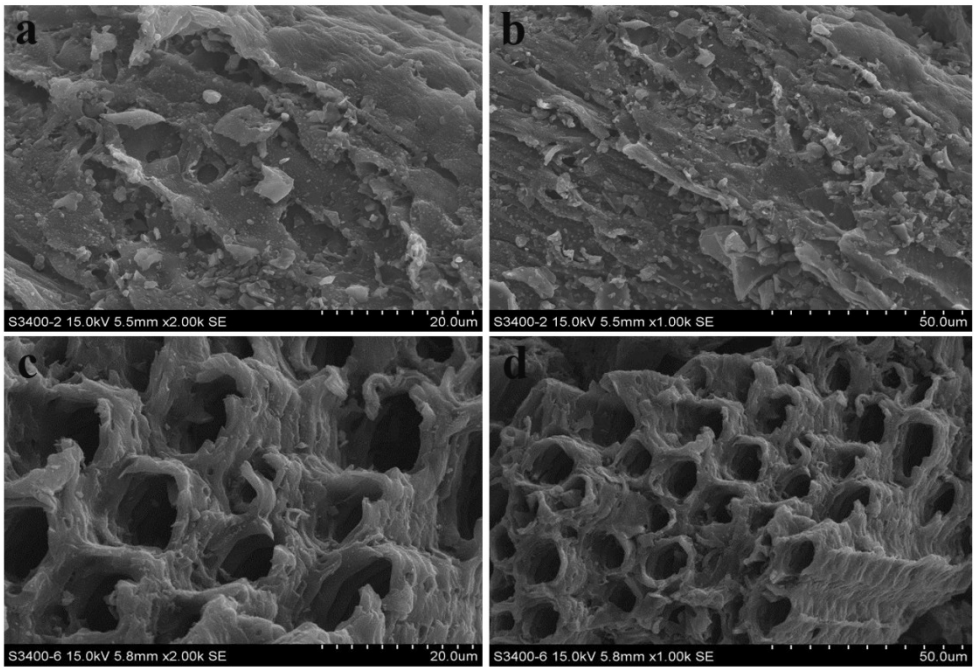

Fig. 4. SEM images of selected corn cob biochar; CK. 2: (a) and (b), Cat. 6: (c) and (d).

thick (2–4 μm) pore walls. However, the morphology of the CK. 2 biochar sample (Figs. 4(a) and 4(b)) is very different. After acid modification, regular and orderly channels can be clearly seen on the SEM images of the Cat. 6 sample (Figs. 4(c) and 4(d)). It can be inferred from this result that the higher pyrolysis temperature and acid treatment were beneficial to the formation of biochar pore channels in the corn cob.

Fig. 5 shows the SEM micrographs of lotus leaf biochar samples before and after acid modification. As can be seen from these images (Figs. 5(a) and 5(b)), the CK. 3 sample surface appears to be a porous, folded structure with attached carbon material debris. After acid modification, it appeared that the surface of the Cat. 7 sample (Figs. 5(c) and 5(d)) had changed exhibiting more cavities with less debris on the acid modified lotus leaf biochar. In addition, the acid modified Cat. 7 had more folds and layers than the unmodified sample. Huang *et al.* also prepared a lotus-leaf-based carbon without acid modification that produced a carbonaceous product without channels and cavities (Huang *et al.*, 2018). It may be that the oxidation reactions induced by the acid produced a porous structure and removed the debris and impurities from the lotus-leaf biochar. Considering that the $DeNO_x$ performance of the lotus leaf biochar improved after acid modification, it is apparent that less debris and abundant channels and cavities on the surface of biochar may be the reason for the improved catalytic performance of the product.

BET Analysis

The specific surface area, pore volume, and pore size distribution of the biochar materials are listed in Table 7. For the three unmodified biochar material, their specific surface area and pore volume were less than 22.00 $m^2\ g^{-1}$ and 0.06 $cm^3\ g^{-1}$ respectively, which was less than the values for the acid modified carbon materials with acid modification. These results suggested that the relatively low specific surface area and pore volume of the unmodified materials was connected their low $DeNO_x$ rate. However, average pore size of the unmodified carbon materials was relatively large and the overall level of the average pore size of these modified carbon materials was much smaller than the pore sizes of the unmodified carbons. This suggested that the acid oxidation acid of the biochar produced smaller pores in the modified carbon.

In contrast to raw carbon materials, after acid modification, the specific surface area and pore volume of the acid modified carbon materials were both higher than 110.00 $m^2\ g^{-1}$ and 0.09 $cm^3\ g^{-1}$ respectively. The highest and lowest the specific surface area was found in the Cat. 5 sample (409.67 $m^2\ g^{-1}$) and Cat. 6 sample (115.24 $m^2\ g^{-1}$), which were derived from corn cob. These results suggested that the physical indices of the corn biochar were greatly affected by the conditions of the acid modification (i.e., acid type, dosage of acid, etc.). In the case of the samples with a good $DeNO_x$ rate (Cat. 6: 22.12% and Cat.7: 21.15%), the specific surface area (Cat. 6: 115.24 $m^2\ g^{-1}$ and Cat.7: 211.88 $m^2\ g^{-1}$) and pore volume (Cat.6: 0.110 $cm^3\ g^{-1}$ and Cat.7: 0.157 $cm^3\ g^{-1}$) of these two samples was not the highest. However, the average pore size of these two samples was relatively high. This suggested that the $DeNO_x$ performance of carbon materials was also related to other factors including surface chemical functionality. Other researchers have also reported that the $DeNO_x$ rate of carbon materials is dependent on surface chemistry (Ren *et al.*, 2017; Yu *et al.*, 2017a). To sum up, the acid modification process changed the physical properties of the carbon materials, and these changes appeared to improve the SCR performance of the resulting carbon material products.

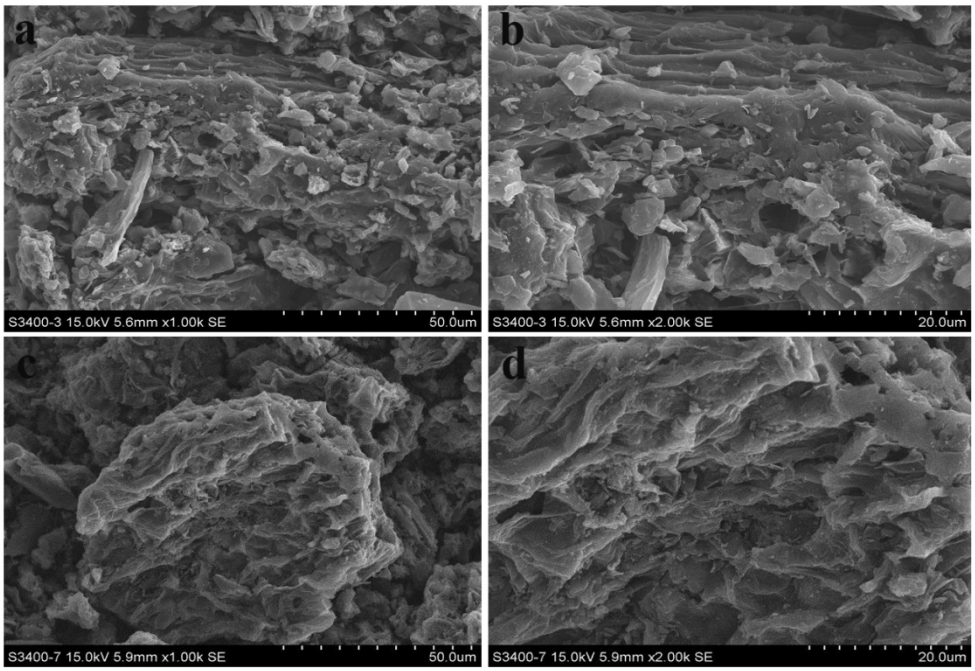

Fig. 5. SEM images of selected lotus leaf biochar; CK. 3: (a) and (b), Cat. 7: (c) and (d).

Table 7. BET data for the biochar material.

Sample	S_{BET} (m^2 g^{-1})	V_{total} (cm^3 g^{-1})	Average pore size (Å)
Cat. 1	218.370	0.140	2.550
Cat. 2	116.680	0.092	3.167
Cat. 3	321.310	0.185	2.299
Cat. 4	312.700	0.110	2.311
Cat. 5	409.670	0.206	2.009
Cat. 6	115.240	0.110	3.816
Cat. 7	211.880	0.157	3.580
Cat. 8	174.630	0.102	2.332
Cat. 9	137.100	0.093	2.720
CK. 1	21.680	0.052	9.647
CK. 2	1.554	0.014	22.150
CK. 3	2.412	0.054	22.642

FT-IR Analysis

To better understand the effect of acid modification on the surface chemical functional groups of the carbon materials, the experimental carbons were subjected to FTIR analysis. The FT-IR results for the experimental carbon materials with and without acid modification are shown in Figs. 6, 7 and 8. Based on previous studies (Gao and Moffat, 1995; Dandekar *et al.*, 1998; Guo *et al.*, 2015; Yu *et al.*, 2015; Ren *et al.*, 2017), the FT-IR bands at 3500–3200 cm^{-1} were due to OH stretching vibrations; the FT-IR bands at 1585cm^{-1} was attributed to the C=C stretching vibration in aromatic compounds; the FT-IR bands at about 1093 cm^{-1}, 797 cm^{-1} and 460 cm^{-1} appeared to be due to Si-O-Si stretching vibration and the FT-IR bands at 973 cm^{-1} were attributed to P-OH species.

The FTIR spectra of selected rice straw biochar samples prepared by different modification parameters are shown given in Fig. 6. As can be seen in Fig. 6, the peak at 1585 cm^{-1} is corresponds to the C=C stretching vibration in aromatic compounds. This suggests that the aromatic compounds in the rice straw did not completely decompose at this relatively low pyrolysis temperature. Consequently, trace amounts of aromatic compounds remained in the Cat.1 sample, which produced an absorbance peak at around 1600 cm^{-1}. Three additional peaks at about 1093 cm^{-1}, 797 cm^{-1} and 460 cm^{-1} appeared to be due to Si-O-Si stretching vibration. The presence of Si in the rice straw biochar is understandable, because Si promotes the growth of rice. The CK. 1 sample was not acid modified, and the absorbance bands at 1093 cm^{-1} and 797 cm^{-1} were not present in the FTIR spectra of the CK. 1 sample. Therefore, it was concluded that some Si could be retained in the biochar after acid modification.

The FTIR spectra of select corn cob biochar samples prepared by different modification parameters are shown in Fig. 7. As can be seen in Fig. 7, broad absorbance bands appeared at about 3400–3500 cm^{-1}, which were assigned to

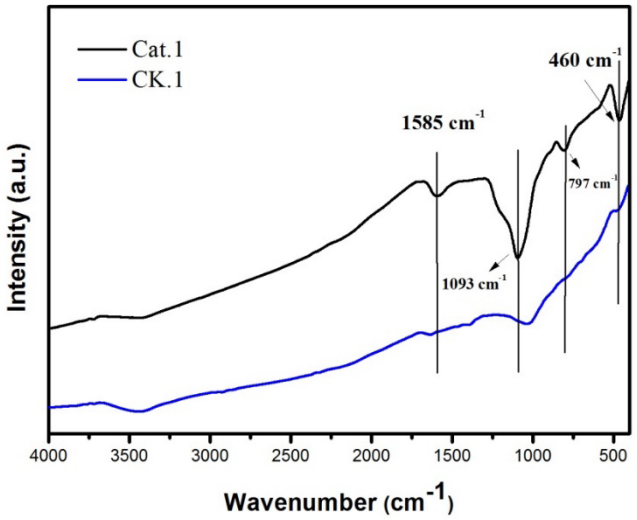

Fig. 6. FT-IR spectra of the selected rice straw biochar samples.

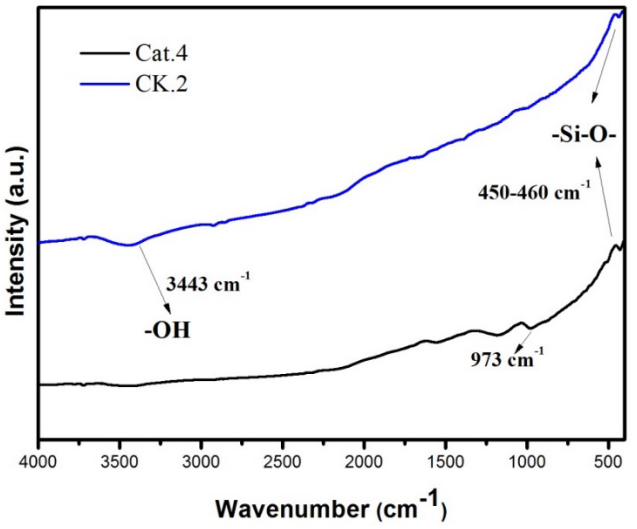

Fig. 7. FT-IR spectra of the selected corn cob biochar samples.

the O-H stretching vibration of the hydroxyl functional groups. The absorbance band that appeared at 973 cm^{-1} in spectrum of the Cat. 4 sample may have been due to the stretching vibration of P-OH species. The band at around 450–460 cm^{-1} could be attributed to the Si-O-Si stretching vibration. After acid modification, it was concluded infer that some Si-O-Si species was retained in the material after acid modification.

The FTIR spectra of selected lotus leaf biochar samples prepared by different modification parameters are shown in Fig. 8. As can be seen in Fig. 8, the broad band at about 3400–3500 cm^{-1} in all the spectra was due to the O-H stretching vibration of the hydroxyl functional groups. The peaks at 1585 cm^{-1} and 1430 cm^{-1} correspond to the C=C stretching vibration in aromatic compounds and COH in-plane bending modes respectively. Compared to samples CK. 3 and Cat. 7, it was found that after acid modification the -COOH

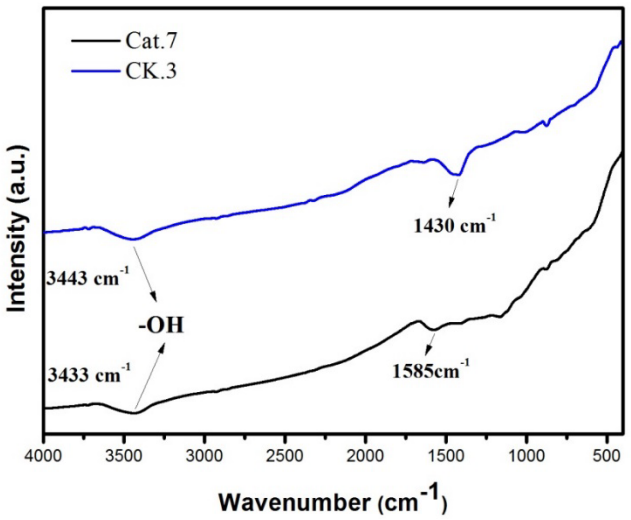

Fig. 8. FT-IR spectra of the selected lotus leaf biochar samples.

related functional groups were present, and the C=C functional groups disappeared. In addition, the intensity of the absorbance of the -COOH related functional groups for Cat. 7 sample was higher than CK. 3. Considering that the NO_x removal rate of Cat.7 was much higher than the CK. 3, it was concluded that the appearance of -COOH groups after acid modification may be a reason for the increase of NO_x removal rate of Cat. 7.

Fig. 1 shows the high NO_x removal rate of Cat. 7, which may be related to the fact that this catalyst had two surface functional groups (-COOH and -OH). Also, the carboxyl, anhydride and phenol groups have also been shown to be responsible for promoting NH_3 adsorption during the $DeNO_x$ process (Zhou *et al.*, 2007; Guo *et al.*, 2015). To summarize, after acid modification, there was an increase in variety and quantity of surface acidic functional groups on the biochar, which improved the adsorption of NH_3. The $DeNO_x$ performance of acid-modified biochar was significantly improved, which may be due to the change of physical and chemical properties of the carbon material after acid modification.

Low Temperature SCR Performance of the Supported Biochar Catalysts

Orthogonal experimental results suggested that the optimum preparation conditions for the biochar materials were biochar carbon material, nitric acid, an acid/mass ratio of 1.50 and a pyrolysis temperature of 800°C. It has been well documented over the past several years that MnO_x based catalysts provide high low temperature SCR performance compared with other metal oxides (Liu *et al.*, 2016; Lee *et al.*, 2017; Liu *et al.*, 2017). In this reported work, the optimum carbon biochar material was used as a carrier to support the active catalyst component (MnO_x). The low temperature $DeNO_x$ performance of the LBC based catalysts with different Mn loading (theoretical load: 0–15%) is shown in Fig. 9 as a function of temperature. The 10% Mn/LBC catalysts exhibited the best low temperature SCR performance in comparison to the other sample catalysts. The highest the NO_x conversion

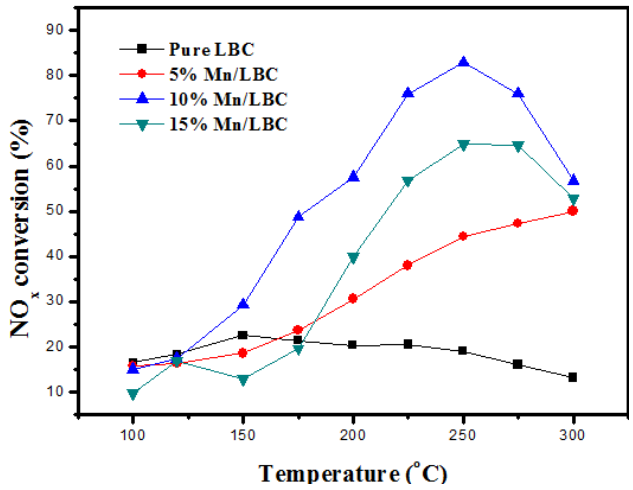

Fig. 9. Low temperature SCR performance for Mn/LBC with different Mn loading.

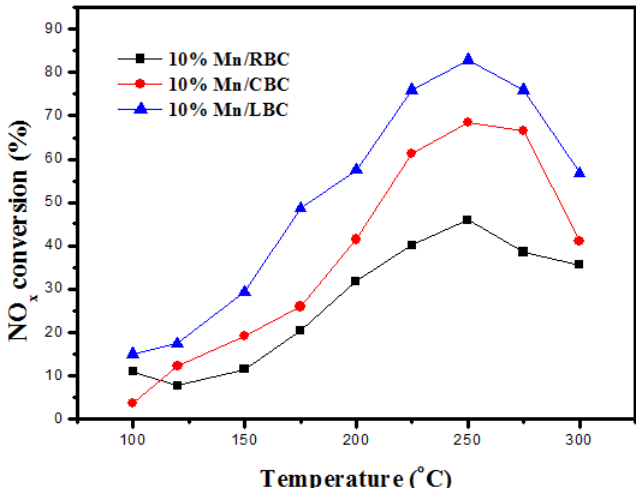

Fig. 10. Low temperature SCR performance for three kinds of biochar supported MnO_x

values of the 10% Mn/LBC catalysts was achieved when the reaction temperature was 250°C. This performance is slightly better than results reported in the literature (Cha *et al.*, 2010; Shen *et al.*, 2015). Below 250°C, the activity of the catalyst increased monotonously with the reaction temperature, and when the reaction temperature was higher than 250°C, the SCR activity of the 10%Mn/LBC catalysts began to decrease. A similar phenomenon has also been observed in the studies of Wang *et al.* (2012) and Su *et al.* (2013). This is because the oxidation of NH_3 readily occurs on the surface of the catalyst at relatively high temperatures. However, the highest NO_x conversion values of 5% for the Mn/LBC and 15% for the Mn/LBC catalysts were both lower than 70%, which may have been related to chemical state of Mn and surface acidity of the catalysts.

Yang *et al.* (2018) used peanut shell bio-char as a support for manganese oxide to form an SCR catalyst and evaluated its activity. Their results showed that the NO_x conversion rate of this catalyst was about 80% at 250°C. A Mn loading of 10 wt% on the biochars reported in this current study was found to be mainly responsible for the observed $DeNO_x$ rate, which was better than that detailed in previously reported work (Singh *et al.*, 2013; Yang *et al.*, 2018).

Finally, the SCR activities as a function of temperature of the 10% Mn/RBC, 10% Mn/CBC and 10% Mn/LBC catalysts were obtained, as shown in Fig. 10. The best low temperature SCR performance of these three samples was also found in the 10% Mn/LBC catalysts. The low temperature SCR performance of the other two catalysts was relatively low, which was less than 75% NO_x conversion.

Characterization of Catalysts

SEM Analysis

Surface morphologies of lotus leaf biochar and 10% Mn/LBC catalyst are shown in Figs. 11(a) and 11(b) and the EDX results for the 10% Mn/LBC catalyst are also presented in Figs. 11(c) and 11(d). As shown by these results, the surface of the lotus leaf biochar prepared by acid modification was relatively clean and the structure was quite porous which favored gas adsorption and reaction. When compared to the material shown in Figs. 11(a) and 11(b), it can be seen that when the modified lotus leaf biochar was loaded with MnO_x its surface roughened, possibly as a result of the dispersion of the active component and the subsequent calcination process. Moreover, many fragments or granular materials appear on the surface of the lotus leaf biochar after loaded with active MnO_x. This phenomenon could be attributed to the active component (MnO_x) supported on the surface of biochar as confirmed by the EDX results (Figs. 11(c) and 11(d)). Also, as illustrated in Figs. 11(c) and 11(d), the mass fraction of manganese in selected areas was about 21.8%, which suggests that dispersion process was efficient and manganese oxide dispersed on the surface of biochar carrier.

H_2-TPR Analysis

H_2-TPR tests were conducted on the 10% Mn/RBC, 10% Mn/CBC and 10% Mn/LBC catalysts to determine the reducibility of metal species in the catalyst and the results are shown in Fig. 12. As shown in this figure, the Mn/biochar catalysts exhibited two redox peaks at 360–380°C and 540–560°C, which correspond to the reduction of MnO_2 or Mn_2O_3 to Mn_3O_4, and Mn_3O_4 to MnO, respectively (Su *et al.*, 2013). A very weak shoulder peak at about 230~230°C was also found and was attributed to the reduction of the easily reducible surface oxygen species (Yu *et al.*, 2017b). Often, the redox ability of a catalyst is closely associated with its low temperature SCR activity, and the stronger the redox capability, the higher the SCR activity (Zuo *et al.*, 2014; Liu *et al.*, 2019; Wang *et al.*, 2020). Comparing the peak positions of these biochar catalysts (Fig. 12), the temperature (336°C) that corresponds to the center of reduction peak of the 10% Mn/LBC catalyst was lower than that of the other catalysts which was an indication of the good low-temperature SCR activity of the 10% Mn/LBC catalyst. Also, the center of reduction peak of the 10% Mn/LBC catalyst was much lower than that of the other bio-char catalysts as reported by Wu *et al.* (2012). Moreover, the temperature that corresponded to the reduction peak center for these catalysts (10% Mn/LBC

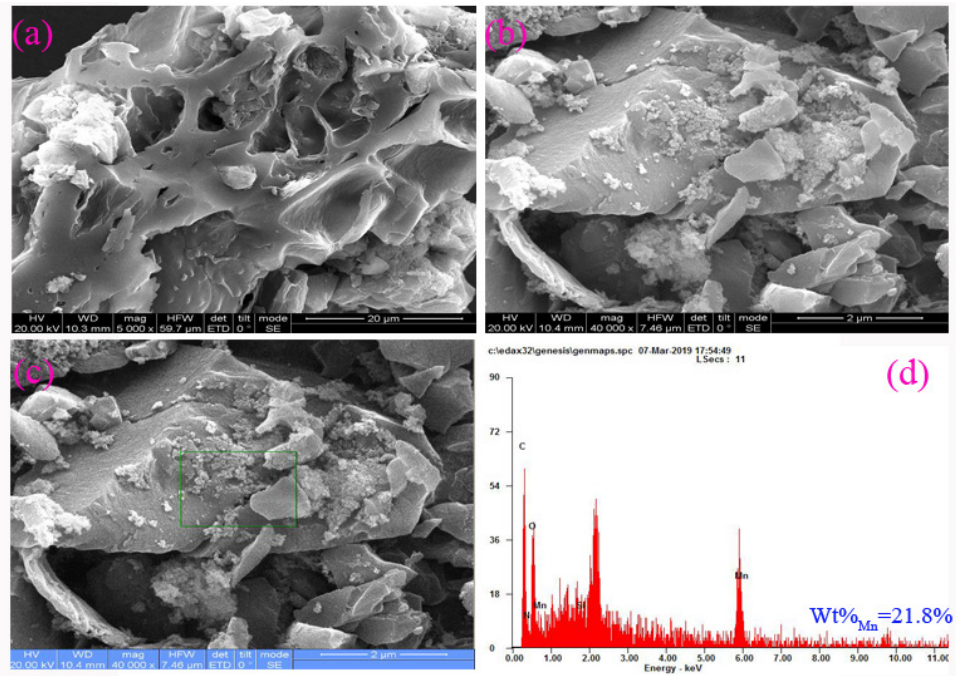

Fig. 11. SEM results of the (a) lotus leaf bio-char and ((b), (c) and (d)) 10% Mn/LBC catalyst.

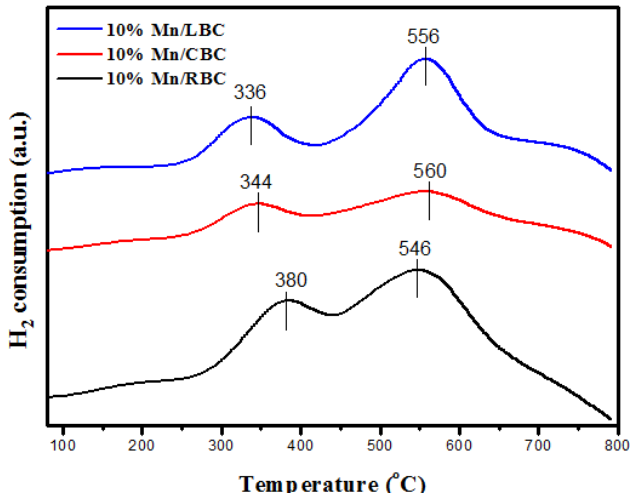

Fig. 12. H_2-TPR results for three kinds of biochar supported 10% Mn catalysts.

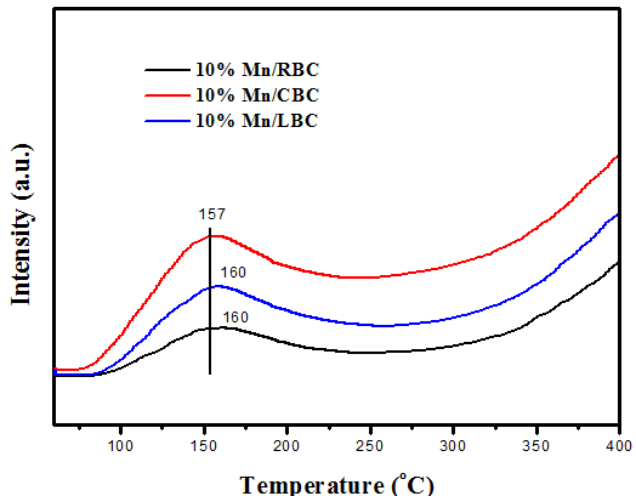

Fig. 13. NH_3-TPD results for three kinds of biochar supported 10%Mn catalysts.

< 10% Mn/CBC < 10% Mn/RBC) could be correlated to the low temperature SCR activity of these catalysts (10% Mn/LBC > 10% Mn/CBC > 10% Mn/RBC).

NH_3-TPD Analysis

The capacity of a catalyst to adsorb NH_3 or activate NH_3 is an important mechanism in the low temperature $DeNO_x$ process (Bosch, 1988; Busca *et al.*, 1998; Chen *et al.*, 2018), and is thought to be governed by respective presence of Lewis and Brönsted acid sites. Fig. 13 shows the NH_3-TPD results of the three types of biochar supported 10% Mn catalysts where it can be seen that the biochar based catalysts appeared to exhibit similar NH_3 desorption curves. The amount of NH_3 adsorbed by the catalysts was in the order of: 10% Mn/CBC > 10% Mn/LBC > 10% Mn/RBC. It was noted that there was a shift in the peak positions of the various catalysts, from which it was concluded that the acid strength of the 10% Mn/CBC catalysts decreased slightly. However, the amount of acid sites of the 10% Mn/CBC catalysts was the highest, while the amount of acid sites of the 10% Mn/RBC catalysts was the lowest, which was obtained by calculating the area under the desorption peaks. Also, the amount of acid sites of 10% Mn/LBC was between that of 10% Mn/CBC and 10% Mn/RBC. Considering the SCR activities of these catalysts, it was suggested that that a suitable surface acidity of the catalysts was one of important reasons for the good SCR performance of supported Mn-based catalysts at low temperature. Comprehensive analysis of the

surface acidity and redox performance of the biochar based catalysts, it shows that the redox performance of each catalyst is relatively different and the catalyst with stronger redox performance has better SCR performance at low temperature. This is consistent with the conclusion that redox capacity of the catalyst is the key to ensure the low temperature activity of the catalyst, which is has been reported in many literatures (Li *et al.*, 2011; Jiang *et al.*, 2019a, b; Wang *et al.*, 2019).

H_2O Resistance Test

Recently, low temperature NH_3-SCR catalysts, such as Mn based catalysts, have attracted the attention of an increasing number of researchers, because they are suitable for a tailend position that can protect catalysts from high concentration of dust (Tong *et al.*, 2020). However, water tolerance of the catalyst is a newly identified problem, which can be ignored at high temperature (Jiang *et al.*, 2018; Han *et al.*, 2019; Wang *et al.*, 2019; Zhang *et al.*, 2019). Therefore, water tolerance tests were performed on the 10% Mn/RBC, 10% Mn/CBC and 10% Mn/LBC catalysts and the results as a function of time are shown in Fig. 14. As shown in this figure, the NO_x conversion of the 10% Mn/LBC catalysts attained a stable level of about 79.0% and proceeded for more than 120 min. However, The NO_x conversion of the other two catalysts decreased with the amount of H_2O (8 vol%) in the inlet gas, where the SCR activity of the 10% Mn/RBC, 10% Mn/CBC decreased from 45% to 33% and from 68% to 53% respectively. However, the $DeNO_x$ rates quickly recovered after the H_2O was removed from the inlet gas. This shows the recoverable activity of the catalysts in the low temperature SCR system. Consequently, it can be concluded from these results that the inhibition effect of H_2O was attributed to the competitive adsorption of H_2O and NH_3 onto the catalyst surface. The possible reasons for this phenomenon were: (1) the active MnO_x in the 10% Mn/LBC catalysts was high dispersed, which allowed for more active sites in NH_3-SCR reaction; and (2) carbon material itself possessed significant hydrophobicity. To summarize, the 10% Mn/LBC catalysts offered better resistance to H_2O than the catalysts.

CONCLUSIONS

In this reported work, the main conclusions were as follows:

(1) The optimum preparation conditions for biochar were successfully determined using an orthogonal experiment L9 (3^4). After acid modification, the changes of surface physics and chemical characteristics of the biochar material appeared to improve the $DeNO_x$ rates of the material. The optimum carbon material was found to be lotus leaf that was treated with nitric acid (acid/mass ratio of 1.50) and pyrolyzed at a temperature of 800°C. The $DeNO_x$ rate of the lotus leaf biochar prepared using the optimum preparation parameters was as high as 22.5%. A select specific surface area and larger pore size played important roles in the $DeNO_x$ process, but the other factors also impacted the low temperature SCR performance of the material. The significance order of the three factors was: A3 (carbon materials type, lotus leaf) > C3 (acid type, nitric acid) > D2 (acid/mass ratio, 1.50) > B3 (pyrolysis temperature, 800°C). Overall, acid modification played an important role in improving SCR activity of biochar materials.

(2) Using agricultural wastes to prepare biochars, and this optimized carbon material was used as the carrier for an active component (MnO_x). The 10% Mn/LBC catalysts were prepared by the ultrasonic impregnation method. The 10% Mn/LBC catalyst exhibited nearly 90% NO_x conversion at 250°C at a high space velocity of 45,000 h^{-1}, but also provided strong H_2O resistance at a reaction temperature of 250°C.

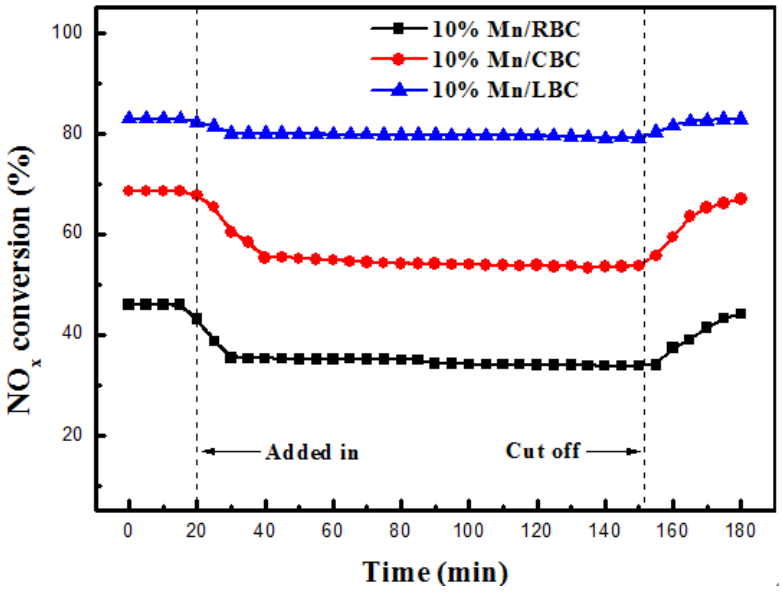

Fig. 14. Effect of H_2O on SCR activity of catalysts: reaction conditions: 0.06% NO, 0.06% NH_3, 2.5% O_2, 8% H_2O, 250°C, Ar balance.

ACKNOWLEDGEMENT

The research was financially supported by the National Natural Science Foundation of China (NSFC-51808269, NSFC-51508245), the Natural Science Foundation of Jiangxi Province (20192BAB213020), the Open Fund of Key Laboratory of Ministry of Education and Research Project of Jiangxi Provincial Education Department (Grant No. GJJ170300).

REFERENCES

Ahmad, N., Ibrahim, N., Ali, U.F.M., Yusuf, S.Y. and Ridwan, F.M. (2016). Carbon-supported CuO catalyst prepared from oil palm empty fruit bunch (EFB) for low-temperature no removal. *Procedia Eng.* 148: 823–829.

Anenberg, S.C., Schwartz, J., Shindell, D., Amann, M., Faluvegi, G., Klimont, Z., Janssens-Maenhout, G., Pozzoli, L., Van Dingenen, R., Vignati, E., Emberson, L., Muller, N.Z., West, J.J., Williams, M., Demkine, V., Hicks, W.K., Kuylenstierna, J., Raes, F. and Ramanathan, V. (2012). Global air quality and health co-benefits of mitigating near-term climate change through methane and black carbon emission controls. *Environ. Health Perspect.* 120: 831–839.

Bai, S.L., Zhao, J.H., Wang, L. and Zhu, Z.P. (2010). SO_2-promoted reduction of NO with NH_3 over vanadium molecularly anchored on the surface of carbon nanotubes. *Catal. Today* 158: 393–400.

Boehm, H.P. (2002). Surface oxides on carbon and their analysis: A critical assessment. *Carbon* 40: 145–149.

Bosch, H. and Jamssen, F. (1988). Formation and Control of Nitrogen Oxide. *Catal. Today* 2: 369–379.

Busca, G., Lietti, L., Ramis, G. and Berti, F. (1998). Chemical and mechanistic aspects of the selective catalytic reduction of NO_x by ammonia over oxide catalysts: A review. *Appl. Catal., B* 18: 1–36.

Cha, J.S., Choi, J.C., Ko, J.H., Park, Y.K., Park, S.H., Jeong, K.E., Kim, S.S. and Jeon, J.K. (2010). The low-temperature SCR of NO over rice straw and sewage sludge derived char. *Chem. Eng. J.* 156: 321–327.

Chen, M.Y., Tsai, Y.C., Tseng, C.F., Lin, H.P. and Hsi, H.C. (2019). Using rice-husk-derived porous silica modified with recycled Cu from industrial wastewater and Ce to remove Hg^0 and NO from simulated flue gases. *Aerosol Air Qual. Res.* 19: 2557–2567.

Chen, Y.R., Wang, M.X., Du, X.S., Ran, J.Y., Zhang, L. and Tang, D.L. (2018). High resistance to Na poisoning of the V_2O_5-$Ce(SO_4)_2/TiO_2$ catalyst for the NO SCR reaction. *Aerosol Air Qual. Res.* 18: 2948–2955.

Cheng, N.L., Li, Y.T., Sun, F., Chen, C., Wang, B.Y., Li, Q., Wei, P. and Cheng, B.F. (2018). Ground-level NO_2 in urban Beijing: Trends, distribution, and effects of emission reduction measures. *Aerosol Air Qual. Res.* 18: 343–356.

Dandekar, A., Baker, R.T.K. and Vannice, M.A. (1998). Characterization of activated carbon, graphitized carbon fibers and synthetic diamond powder using TPD and DRIFTS. *Carbon* 36: 1821–1831.

Dong, L., Fan, Y., Ling, W., Yang, C. and Huang, B. (2017). Effect of Ce/Y addition on low-temperature SCR activity and SO_2 and H_2O resistance of MnO_x/ZrO_2/MWCNTs catalysts. *Catalysts* 7: 181.

Fu, M.F., Li, C.T., Lu, P., Qu, L., Zhang, M.Y., Zhou, Y., Yu, M.G. and Fang, Y. (2014). A review on selective catalytic reduction of NO_x by supported catalysts at 100–300°C—catalysts, mechanism, kinetics. *Catal. Sci. Technol.* 4: 14–25.

Gao, S. and Moffat, J.B. (1995). An infrared spectroscopy study of 1-butene and its isomers adsorbed onto 12-tungstophosphoric AcidSiO_2. *Colloids Surf., A* 105: 133–142.

Guo, Q.Q., Jing, W., Hou, Y.Q., Huang, Z.G., Ma, G.Q., Han, X.J. and Sun, D.K. (2015). On the nature of oxygen groups for NH_3-SCR of NO over carbon at low temperatures. *Chem. Eng. J.* 270: 41–49.

Han, L., Cai, S., Gao, M., Hasegawa, J.Y., Wang, P., Zhang, J., Shi, L. and Zhang, D. (2019). Selective catalytic reduction of NO_x with NH_3 by using novel catalysts: State of the art and future prospects. *Chem. Rev.* 119: 10916–10976.

Huang, H.B., Wang, Y., Jiao, W.B., Cai, F.Y., Shen, M., Zhou, S.G., Cao, H.L., Lu, J. and Cao, R. (2018). Lotus-leaf-derived activated-carbon-supported nano-CdS as energy-efficient photocatalysts under visible irradiation. *ACS Sustainable Chem. Eng.* 6: 7871–7879.

Huang, M.C. and Teng, H.S. (2003). Nitrogen-containing carbons from phenol–formaldehyde resins and their catalytic activity in NO reduction with NH_3. *Carbon* 41: 951–957.

Huang, Y., Su, W.H., Wang, R. and Zhao, T.S. (2019). Removal of typical industrial gaseous pollutants: From carbon, zeolite, and metal-organic frameworks to molecularly imprinted adsorbents. *Aerosol Air Qual. Res.* 19: 2130–2150.

Jiang, Y., Bao, C.Z., Liu, S.J., Liang, G.T., Lu, M.Y., Lai, C.Z., Shi, W.Y. and Ma, S.Y. (2018). Enhanced Activity of Nb-modified CeO_2/TiO_2 catalyst for the selective catalytic reduction of NO with NH_3. *Aerosol Air Qual. Res.* 18: 2121–2130.

Jiang, Y., Lai, C.Z., Liu, S.J., Liang, G.T., Bao, C.Z., Shi, W.Y. and Ma, S.Y. (2019a). Deactivation of Ce-Ti oxide catalyst by K_3PO_4 for the selective catalytic reduction of NO with NH_3. *Aerosol Air Qual. Res.* 19: 422–430.

Jiang, Y., Shi, W.Y., Lu, M.Y., Li, Q.Y., Lai, C.Z., Gao, W.Q., Yang, L. and Yang, Z.D. (2019b). Enhanced low-temperature NH_3-SCR activity over Ce-Ti oxide catalysts by hydrochloric acid treatment. *Aerosol Air Qual. Res.* 19: 2381–2386.

Jiao, J.Z., Li, S.H. and Huang, B.C. (2015). Preparation of manganese oxides supported on graphene catalysts and their activity in low-temperature NH_3-SCR. *Acta Phys. Chim. Sin.* 31: 1383–1390.

Jo, Y.B., Cha, J.S., Ko, J.H., Shin, M.C., Park, S.H., Jeon, J.K., Kim, S.S. and Park, Y.K. (2011). NH_3 selective catalytic reduction (SCR) of nitrogen oxides (NO_x) over activated sewage sludge char. *Korean J. Chem. Eng.* 28: 106–113.

Lee, T.Y., Liou, S.Y. and Bai, H.L. (2017). Comparison of titania nanotubes and titanium dioxide as supports of low-

temperature selective catalytic reduction catalysts under sulfur dioxide poisoning. *J. Air Waste Manage. Assoc.* 67: 292–305.

Li, J.H., Chang, H.Z., Ma, L., Hao, J.M. and Yang, R.T. (2011). Low-temperature selective catalytic reduction of NO_x with NH_3 over metal oxide and zeolite catalysts—A review. *Catal. Today* 175: 147–156.

Liu, C., Shi, J.W., Gao, C. and Niu, C.M. (2016). Manganese oxide-based catalysts for low-temperature selective catalytic reduction of NO_x with NH_3: A review. *Appl. Catal., A* 522: 54–69.

Liu, H.B., Zhang, Z.X., Li, Q., Chen, T.H., Zhang, C.G., Chen, D., Zhu, C.Z. and Jiang, Y. (2017). Novel method for preparing controllable nanoporous α-Fe2O_3 and its reactivity to SCR De-NO_x. *Aerosol Air Qual. Res.* 17: 1898–1908.

Liu, S.J., Ji, P.D., Ye, D., Qu, R.Y., Zheng, C.H. and Gao, X. (2019). Regeneration of potassium poisoned catalysts for the selective catalytic reduction of NO with NH_3. *Aerosol Air Qual. Res.* 19: 649–656.

Lu, P., Li, C.T., Zeng, G.M., He, L.J., Peng, D.L., Cui, H.F., Li, S.H. and Zhai, Y.B. (2010). Low temperature selective catalytic reduction of NO by activated carbon fiber loading lanthanum oxide and ceria. *Appl. Catal., B* 96: 157–161.

Marban, G., Valdes-Solis, T. and Fuertes, A.B. (2004). Mechanism of low-temperature selective catalytic reduction of NO with NH_3 over carbon-supported Mn_3O_4: Role of surface NH_3 species: SCR mechanism. *J. Catal.* 226: 138–155.

Mu, L., Zheng, L.R., Liang, M.S., Tian, M., Li, X.M. and Jing, D.H. (2019). Characterization and source analysis of water-soluble ions in atmospheric particles in Jinzhong, China. *Aerosol Air Qual. Res.* 19: 2396–2409.

Peng, X., Ye, L.L., Wang, C.H., Zhou, H. and Sun, B. (2011). Temperature- and duration-dependent rice straw-derived biochar: Characteristics and its effects on soil properties of an Ultisol in southern China. *Soil Tillage Res.* 112: 159–166.

Ren, S., Guo, F.Q., Yang, J., Yao, L., Zhao, Q. and Kong, M. (2017). Selection of carbon materials and modification methods in low-temperature sintering flue gas denitrification. *Chem. Eng. Res. Des.* 126: 278–285.

Samojeden, B., Motak, M. and Grzybek, T. (2015). The influence of the modification of carbonaceous materials on their catalytic properties in SCR-NH_3. A short review. *C.R. Chim.* 18: 1049–1073.

Shen, B.X., Chen, J.H., Yue, S.J. and Li, G.L. (2015). A comparative study of modified cotton biochar and activated carbon based catalysts in low temperature SCR. *Fuel* 156: 47–53.

Singh, S., Nahil, M.A., Sun, X., Wu, C.F., Chen, J.H., Shen, B.X. and Williams, P.T. (2013). Novel application of cotton stalk as a waste derived catalyst in the low temperature SCR-deNO_x proces. *Fuel* 105: 585–594.

Skalska, K., Miller, J.S. and Ledakowicz, S. (2010). Trends in NO_x abatement: A review. *Sci. Total Environ.* 408: 3976–3989.

Su, Y., Fan, B., Wang, L., Liu, Y., Huang, B., Fu, M., Chen, L. and Ye, D. (2013). MnO_x supported on carbon nanotubes by different methods for the SCR of NO with NH_3. *Catal. Today* 201: 115–121.

Tong, Y.M., Li, Y.S., Li, Z.B., Wang, P.Q., Zhang, Z.P., Zhao, X.Y., Yuan, F.L. and Zhu, Y.J. (2020). Influence of Sm on the low temperature NH_3-SCR of NO activity and H_2O/SO_2 resistance over the SmaMn$Ni_2Ti_7O_x$ (a = 0.1, 0.2, 0.3, 0.4) catalysts. *Appl. Catal., A* 590: 117333.

Wang, H., Huang, B., Yu, C., Lu, M., Huang, H. and Zhou, Y. (2019). Research progress, challenges and perspectives on the sulfur and water resistance of catalysts for low temperature selective catalytic reduction of NO_x by NH_3. *Appl. Catal., A*: 588: 117207.

Wang, L., Huang, B., Su, Y., Zhou, G., Wang, K., Luo, H. and Ye, D. (2012). Manganese oxides supported on multi-walled carbon nanotubes for selective catalytic reduction of NO with NH_3: Catalytic activity and characterization. *Chem. Eng. J.* 192: 232–241.

Wang, Q., Zhou, J., Zhang, J., Zhu, H., Feng, Y. and Jin, J. (2020). Effect of ceria doping on the catalytic activity and SO_2 resistance of MnO_x/TiO_2 catalysts for the selective catalytic reduction of NO with NH_3 at low temperatures. *Aerosol Air Qual. Res.* 20: 477–488.

Wang, S.X. and Hao, J.M. (2012). Air quality management in China: Issues, Challenges, and options. *J. Environ. Sci.-China* 24: 2–13.

Wu, C.F., Nahil, M.A., Sun, X., Singh, S., Chen, J.H., Shen, B.X. and Williams, P.T. (2012). Novel application of biochar from biomass pyrolysis for low temperature selective catalytic reduction. *J. Energy Inst.* 85: 236–239.

Xiao, X., Sheng, Z.Y., Yang, L. and Dong, F. (2016). Low-temperature selective catalytic reduction of NO_x with NH_3 over a manganese and cerium oxide/graphene composite prepared by a hydrothermal method. *Catal. Sci. Technol.* 6: 1507–1514.

Yang, J., Zhou, J., Tong, W., Zhang, T., Kong, M. and Ren, S. (2018). Low-temperature flue gas denitration with transition metal oxides supported on biomass char. *J. Energy Inst.* 92: 1158–1166.

Yu, C.L., Wang, L.S. and Huang, B.C. (2015). *In situ* DRIFTS study of the low temperature selective catalytic reduction of NO with NH_3 over MnO_x supported on multi-walled carbon nanotubes catalysts. *Aerosol Air Qual. Res.* 15: 1017–1027.

Yu, C.L., Chen, F., Dong, L.F., Liu, X.Q., Huang, B.C., Wang, X.N. and Zhong, S.B. (2017a). Manganese-rich MnSAPO-34 molecular sieves as an efficient catalyst for the selective catalytic reduction of NO_x with NH_3: One-pot synthesis, catalytic performance, and characterization. *Environ. Sci. Pollut. Res.* 24: 7499–7510.

Yu, C.L., Dong, L.F., Chen, F., Liu, X.Q. and Huang, B.C. (2017b). Low-temperature SCR of NO_x by NH_3 over MnO_x/SAPO-34 prepared by two different methods: A comparative study. *Environ Technol* 38: 1030–1042.

Yu, S.H., Jiang, N.X., Zou, W.X., Li, L.L., Tang, C.J. and Dong, L. (2016). A general and inherent strategy to improve the water tolerance of low temperature NH_3-SCR catalysts via trace SiO_2 deposition. *Catal. Commun.* 84: 75–79.

Zhang, N.Q., Li, L.C., Zhang, B.B., Sun, Y.M., Song, L.Y., Wu, R. and He, H. (2019). Polytetrafluoroethylene modifying: A low cost and easy way to improve the H_2O resistance ability over MnO_x for low-temperature NH_3-SCR. *J. Environ. Chem. Eng.* 7: 103044.

Zhou, J.H., Sui, Z.J., Zhu, J., Li, P., De, C., Dai, Y.C. and Yuan, W.K. (2007). Characterization of surface oxygen complexes on carbon nanofibers by TPD, XPS and FT-IR. *Carbon* 45: 785–796.

Zhu, L., Huang, B., Wang, W., Wei, Z. and Ye, D. (2011). Low-temperature SCR of NO with NH3 over CeO_2 supported on modified activated carbon fibers. *Catal. Commun.* 12: 394–398.

Zhu, Z.P., Liu, Z.Y., Liu, S.J. and Niu, H.X. (1999). A novel carbon-supported vanadium oxide catalyst for NO reduction with NH_3 at low temperatures. *Appl. Catal., B* 23: L229–L233.

Zuo, J.L., Chen, Z.H., Wang, F.R., Yu, Y.H., Wang, L.F. and Li, X.H. (2014). Low-temperature Selective catalytic reduction of NO_x with NH_3 over novel Mn–Zr mixed oxide catalysts. *Ind. Eng. Chem. Res.* 53: 2647–2655.

Received for review, December 2, 2019
Revised, March 21, 2020
Accepted, March 22, 2020